Energy 311 (2024) 133318

Contents lists available at ScienceDirect

Energy

journal homepage: www.elsevier.com/locate/energy

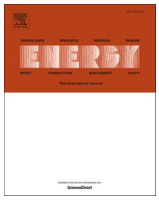

Experimental and theoretical assessment of the effects of electrical load variation on the operability of a small-scale Organic Rankine Cycle (ORC)-based unit equipped with a hermetic scroll expander

Fabio Fatigati *, Roberto Cipollone

University of L'Aquila, Department of Industrial and Information Engineering and Economics, Piazzale Ernesto Pontieri, L'Aquila, 67100, Italy

ARTICLE INFO

KEWORDS:
Solar Organic Rankine cycle (ORC)-Based units
Scroll expander
Micro-cogeneration
Variable electric load
ORC unit control
Variable speed control

ABSTRACT

Scroll expanders are widely adopted in small-scale Organic-Rankine-Cycles-(ORCs)-units integrated with renewable energy sources for low power residential Combined Heat and Power Production (CHP). These expanders are often connected to variable direct loads without the possibility to impose its speed externally. Despite the effect of electric load variation on expander speed is known, a minor attention is focused on its impact on the plant operability and regulation. To fill this gap, a wide experimental analysis is carried out on a solar micro-cogenerative ORC-based power unit equipped with a 1 kW hermetic scroll expander connected with a variable electric load. The experimental behaviour of the ORC-unit was assessed for different values of load resistance (from 20 Ω up to 80 Ω). Results show that properly acting on the load resistance the ORC-power unit can be improved up to 50 % in terms of efficiency and power production. Moreover, if the expander is properly designed its self-regulatory capability allows to achieve similar performance of an equivalent speed-controlled expander tested on the same plant. Finally, a new theoretical model reproducing the impact of main operating quantities on expander behaviour was developed and experimentally validated paving the way to a novel model-based control approach.

1. Introduction

The most important challenge of these recent years is certainly the strong impact of human activities on the climate change, [1]. Therefore, the main driver of the research is the reduction of greenhouse gases emissions, focusing the attention to carbon dioxide CO_2. To pursue this aim a universally agreed common commitment is to achieve a net zero emissions target by 2050, [2–4], eventually compensating the "hard to abate" sectors with Carbon absorption by biomasses. The transition to a zero or to a low-carbon emission economy is synthetised by the so-called Sustainable Development Goals (SDG) of the UN Agenda 2030 which widens the efforts toward a sustainable development which introduces social and economic aspects, as well as a much wider environmental compatibility of human actions. Goals n. 7 and 13 directly address to a CO_2 emissions while n. 12 focus the attention to a responsible consumption and production particularly interesting on the domestic sector. In fact, concerning the energy use in buildings, in 2020 reversed in the atmosphere 2.7 billion of tonnes of CO_2 [5] corresponding to the 17.5 % of the whole total emissions [6]. To reduce its environmental impact, it is fundamental the adoption and a better exploitation of renewable energy sources to replace fossil fuel which still accounting for a share higher than 80 % of the total energy supply [7].

An interesting opportunity for local cogeneration in the residential sector is offered by the integration of Organic Rankine Cycles (ORCs) power unit with pre-existent thermal heating and storage systems based on the exploitation of solar energy. Under this light, ORCs-units are highly competitive for the retrofit of existing solar installation for the domestic hot water (DHW) production, [8]. Also biomass-fired-ORC-unit [9,10] and ORC-geothermal CHP systems [11–13] represent a reliable solution to reduce the fossil fuel utilization, [14]. Generating units based on Organic Rankine Cycles (ORCs) indeed allow to exploit low thermal hot source, thus ensuring an effective cascade utilization of heat with a significant reduction of carbon emission, [14].

Small scale CHP-ORC units frequently operate in severe off design and transient conditions so Thermal Energy Storage (TES) systems are usually adopted, [15] whose aim is to ensure the unpredictable demand of heat and favour a continuous thermal energy recovery during

* Corresponding author.
E-mail address: fabio.fatigati@univaq.it (F. Fatigati).

https://doi.org/10.1016/j.energy.2024.133318
Received 8 July 2024; Received in revised form 2 September 2024; Accepted 29 September 2024
Available online 5 October 2024

daytime. Despite TES employment, ORC-units frequently work far from the design conditions when the electrical energy is produced in absence of solar energy, during night-time or low solar irradiation, [16], discharging the thermal energy stored. This situation applies again when biomasses [17] and geothermal energy [18] are used to feed the unit, due to other constrains concerning the energy availability. Unfortunately, at off-design working conditions, mainly at low load, performances are seriously compromised in terms of efficiency and, therefore, of electrical energy produced. A reduced level of thermal energy feeding the unit, in fact, produces a lack of stability (usually a wet saturated fluid inside the expander), temperature levels among hot and cold sources too close, uncertain starting conditions and, more generally, energy performances degradation, [19]. Main variables which affect a proper working of the unit are: (a) the working fluid mass flow rate; (b) the ORC maximum pressure and temperature; (c) heat available at the hot source and its temperature. To answer to the off design of these quantities, an important literature has been produced in the past years in terms of control strategies of the unit. In Ref. [20] it was seen that a proper control of pump and expander speed allows to overcome the fluctuation of heat source and the best results are achieved regulating the evaporating temperature. In Ref. [21] the main control parameter is the superheating degree at expander inlet, performed through an integration of a feedforward and a classic feedback PI (proportional and integral) regulation action. In this case, main operating parameter was the Working Fluid (WF) mass flow rate while a regulation of the input heat (via the flow rate of a carrying medium) allows to control expander intake pressure. Also, in Ref. [22] the pump speed was chosen to set the WF mass flow rate to achieve a desired evaporating temperature, adding a derivative action to a PI feedback regulation. In Ref. [17] control strategies on superheating degree and shaft power are examined exploiting feedforward and feedback control actions. An interesting result was a response time of 12.3 s and 7.8 s having fixed suitable set up for the superheating degree and shaft power, respectively. Expander speed add a further degree of freedom in the control of superheating degree [20] and expander maximum pressure [23]. If the unit is connected on the grid, expander speed variation can be achieved through a regenerative inverted but the cost of the unit increases, increasing Pay Back Time, PBT, the most important economic parameter to widen the market penetration.

An easier and low-cost arrangement is when the generator (mechanically linked to the expander) is connected to an electric load often represented by a battery. In this case, the expander speed is constrained by the torque balance on the expander shaft, [24], and it cannot be considered as a degree of freedom. For a given electric load value, expander speed increases with WF mass flow rate (because of the increase of the shaft torque imposed by the expander), and consequently with pump speed which supports a greater flow rate delivered. Moreover, for a given pump speed (a given WF mass flow rate), the expander rotates faster when the load impedance increases, [24]. The same conclusion is reached in Ref. [25] where the effects of the electric load variation on the performance of ORC-based unit are assessed. As it was expected from a reversible behaviour, decreasing the electrical load resistance produces a reduction on the expander speed, under constant output power conditions. An increase of expander intake pressure and torque and a decrease of the superheating degree were also observed. In Ref. [26] it was found that as the electric load resistance gets lower, the generated current grows due to the electric generator characteristics (Voltmaster Electric AC Generator, AB30L type, manufactured by WANCO INC), the corresponding torque requested by the generator increases since the proportional relation between its current and torque. By the same authors, in Ref. [26] it was observed that for a fixed rotation speed, the power output of the unit decreases with the increase of electrical load resistance. With an electric load of 20 Ω the power output of the unit was 557 W while for an electrical load equal to 75.5 Ω the power of the unit decreases up to 80 %. Also, in Refs. [27,28] a reduction of the expander speed with the current absorbed by the electric load is observed. Furthermore, an optimum value of the generator output was found as a function of the electric load finding the optimum of the whole unit performance, [29].

All these results were experimentally observed, and no additional efforts were presented from a theoretical approach. Theoretical motivations explaining these results based on physically consistent relationships are still not available. For a more comprehensive theoretical base, other relevant quantities could be linked together with the electrical load variations such as expander maximum pressure, pressure ratio, working fluid (WF) mass flow rate, etc... A theoretical tool able to represent all these operational properties including the load variations would give to the designer a reliable approach to optimize the working condition the unit. Within this aim, even few percentage points of improvement (power produced, efficiency, etc …) would be particularly appreciated considering the limited electrical energy recoverable. A model-based control strategy which includes the electrical motor speed controlled by varying an electrical load could rule the unit to its maximum performance.

To fill this gap, in the present paper, a wide experimental analysis on the behaviour of the solar-assisted ORC-based unit for different electrical load conditions imposed to the generator was deeply assessed. Subsequently, the operating region of the unit on which the speed was varied via the electric load was experimentally compared with the case studied in Ref. [30] where a Sliding Rotary Vane Expander (SRVE) having a similar power size had the speed continuously controlled by a regenerative inverter so, decoupling the connection to the grid with the shaft speed of the expander and electric motor. The comparison allowed to define the pro and cons of the different expander performances and, definitively, efficiency and power produced by the unit. Such analysis allows to discover novel aspects in terms of expander self-regulating capability.

Finally, a theoretical model of the unit which includes the effects of the electrical load variation has been developed and validated. The full unit operability was reproduced, and a robust electrical load control was added together with the others control strategies more oriented to the thermodynamic variables of the unit (i.e. maximum operating pressure)

2. Materials and methods

2.1. Experimental test bench

To deepen the effect of the electric load variation connected to the generator driven by the expander and, consequently, of the plant behaviour including the electricity generation, an in-deep experimental analysis was carried out on a fully instrumented test bench on which a unit was operated. The test bench (Fig. 1) was conceived to be integrated to 15 m^2 flat plate solar collectors (FPTC). The solar section was simulated through the adoption of 2 electric resistances (a) of 12 kW each. Electric resistances provide thermal power to 150 L of water stored in a Thermal Energy Storage (b). Such choice is due to reduce the time to heat up the water thus performing a high quantity of test in a day ensuring proper repeatability of the results. The hot water inside the reservoir is provided through a dedicated pump (c) to the hot side of a Plate Heat Recovery Vapor Generator (PHRVG) (d). Thanks to a regulating valve (e) the hot water flow rate can be set. It provides the thermal power to the Working Fluid (WF) flowing in counter flow on the cold side of the PHRVG. As working fluid, a R245fa is selected and mixed with POE ISOVG68 oil to lubricate the pump and expander. The oil is mixed in a share of 5 % of the mass of the working fluid (5 kg). The working fluid mass flow rate is controlled thanks to a diaphragm pump with a volume displacement of 6.1 cm^3 (f). R245fa was used as working fluid, in spite of the more recent pure fluid (n-Octane, R113, R123, Cyclohexane, and Toluene), [31] or mixture (butane/pentane, hexane/acetone, R1234ze(E)/R245fa), [32,33], to have the possibility to compare the results and appreciate the improvements with respect to previous research which used the R245fa fluid. Moreover, due to the

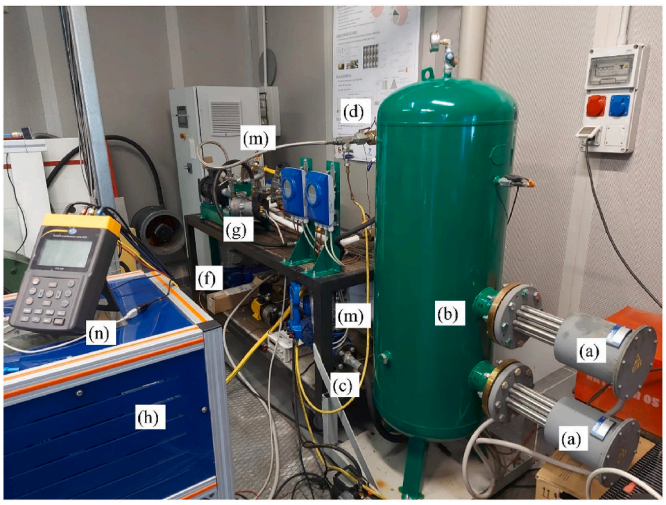

(a)

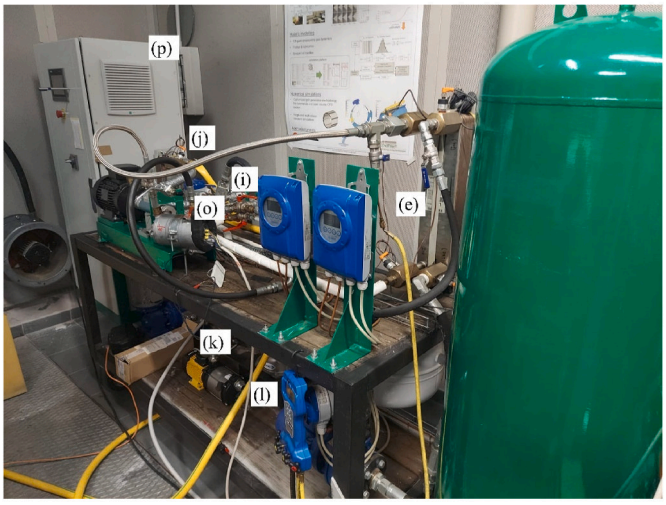

(b)

Fig. 1. Views of ORC-based unit test bench (a) and (b).

high performance when applied to small scale ORC-based power unit [34,35], R245fa is widely adopted in literature giving a wide database for experimental comparison.

Thanks to a dedicated inverter the pump speed can be varied to set a proper mass flow rate which guarantees a superheating degree of the WF at PHRVG outlet between 5 °C and 20 °C according to the thermal power of the heat source. The superheated vapor of WF enters a 1 kW hermetic scroll expander (g), derived by simple arrangements from a compressor. The scroll shares the shaft with a generator and both these components are enclosed in the same casing. The expander is connected to a resistive electric load through an AC/DC converter. Hence, the expander generator produces a three-phase voltage at variable frequency (according to the shaft speed) which is converted in DC voltage by an AC/DC converter and then dissipated on a variable resistive load (h). For the case at hand the electric load was varied from 20 Ω up to 80 Ω. Once a specific value of it is set, the electrical current flowing is known and therefore the electric power dissipated.

The electrical power produced by the generator represents a load for the expander and brings in equilibrium the common shaft. In fact, in steady conditions, the torque produced by the expander must be equal to that requested by the generator, apart from the mechanical losses being the speed the results of the equilibrium of the torques applied to the shaft. Of course, a chain of efficiencies must be considered starting from the electrical power feeding the load. So, the rotating speed of the expander cannot be set directly as it would be more suitable for many reasons.

Concerning scroll expander its intake volume is 12 cm^3 while the built in volume ratio is equal to 2. For the case at hand, the expander speed is not imposed externally through an inverter but depends by the torque equilibrium on the shaft. WF exiting the expander flows in the hot side of Recuperative Heat Exchanger (RHX) (i) before to enters the condenser (j). In this way, it preheats the WF flowing in the cold side of RHX before it enters the PHRVG. This allows to perform a recovery of thermal power which anyway it would be wasted at the condenser. The WF exiting the condenser was gathered in 3 L receiver (k) which has the role to damp the mass flow rate fluctuation and avoid cavitation phenomena being located upstream the pump.

Concerning the measurement instruments (Fig. 2), upstream and downstream each component a pressure and temperature transducers are placed to reconstruct the thermodynamic cycle. The working fluid mass flow rate was measured through a Coriolis Mass flow meter (l) whereas the hot and cold-water flow rate are measured via a magnetic flow meter (m). The expander and pump power are measured by a Wattmeter (n) placed upstream the AC/DC converter while the expander speed thanks to a magnetic probe introduced inside the casing of the machine and reading the results on a dedicated oscilloscope (o) (Fig. 3). Element (p) represent the Electric control unit where the WF and hot water pump speed and the electric resistances are controlled. The uncertainty of measurement of the adopted instrument are reported in Table 1.

The same test bench was used in Ref. [30] considering another expander type. This was a Sliding Rotary Vane Expander, SVRE, mechanically connected with an electric asynchronous generator electrically connected with a 50 Hz network. Thanks to a regenerative inverter the speed of rotation of the expander (and of the electric motor) was externally controlled and considered as a degree of freedom. To analyse the effects of the different configurations on the operating range, the experimental data referred to the case at hand (scroll connected to a

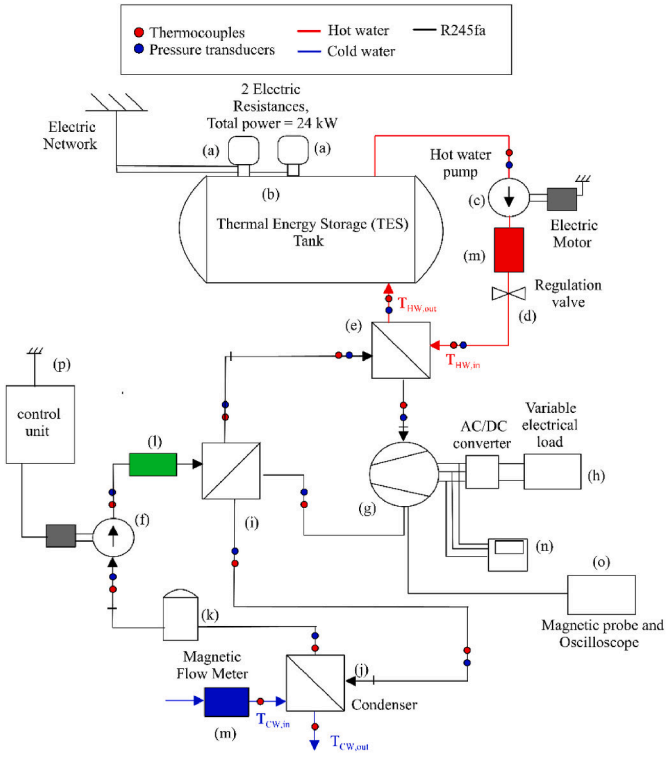

Fig. 2. Scheme of measurements instruments and plant components.

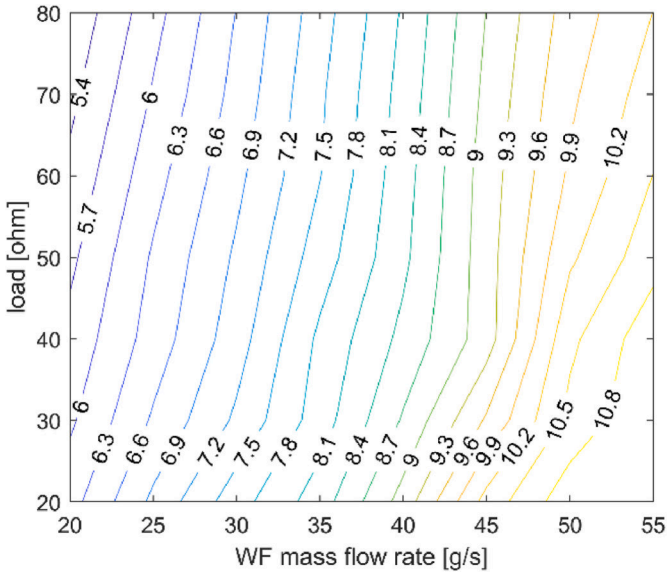

Fig. 3. Experimental expander intake pressure as function of load resistance and mass flow rate of WF.

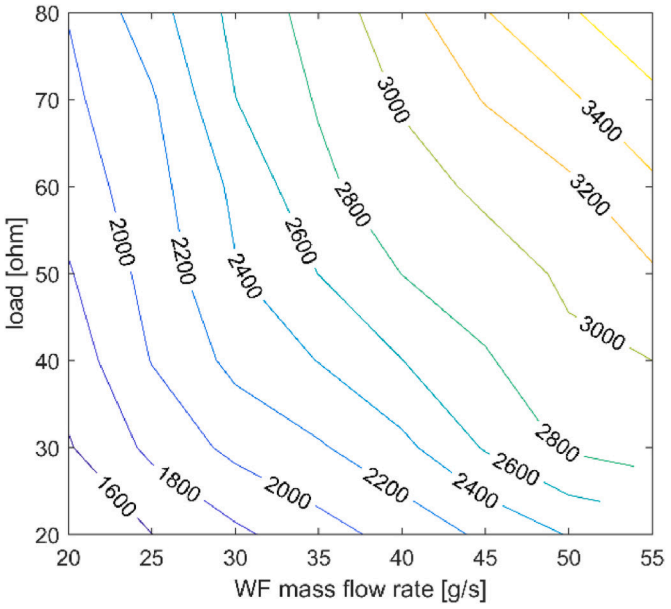

Fig. 4. Experimental expander speed as function of load resistance and mass flow rate of WF.

Table 1
Measurement uncertainty.

Variable	Sensor Type	Measurement uncertainty
Temperature	Thermocouple	±0.75 °C
Pressure	Pressure transducers	±1.5 % of full-scale
Mass flow rate (R245fa)	Magnetic Flow meter	±0.15 % measured value
Mass flow rate (water)	Magnetic Flow meter	±0.5 % measured value
Power	Wattmeter	±1 % measured value

variable load) was compared with that explored in Ref. [30].

3. Results

3.1. Experimental analysis of the effect of the electric load and WF mass flow rate on ORC-based unit operability

To assess the impact of WF mass flow rate and electric load variation on the ORC-based power unit operability, a wide experimental analysis was carried out. The performance of the unit was observed setting an electric load and varying the working fluid mass flow rate according to the thermal power available at evaporator to guarantee a superheating degree between 5 and 20 °C. The analysis was repeated for different values of electric load ranging from 20 Ω up to 80 Ω.

The wide data set allows to outline operating map expressing the main operating quantities as function of electric load (L) and working fluid (WF) mass flow rate. In Fig. 3, it can be seen the expander intake pressure as function of these two parameters. For a fixed L value (y-axis), the expander intake pressure increases with WF mass flow rate in accordance with what seen in Ref. [30]. Keeping constant, instead, the WF mass flow rate (x-axis), it can be observed as the expander intake pressure diminishes when L increases. Observing for instance a working fluid mass flow rate equal to 45 g/s, Fig. 3 shows as a steep expander pressure variation from 10.2 bar up to 9.3 bar is achieved varying L from 20 Ω up to 40 Ω.

Increasing L beyond 40 Ω, a pressure reduction is also observed but its slope is significantly weaker with respect to the one observed for lower L values. This can be noticed also in correspondence of other WF mass flow rates. Indeed, varying L the intake pressure sees a significant variation between 20 Ω and 40 Ω while a weaker reduction is observed for L exceeding 40 Ω. These results can be explained observing Fig. 4 reporting the expander speed as function of WF mass flow rate and L. For a given WF mass flow rate, between 20 Ω and 40 Ω, the expander speed increases as the L increases. The speed increase with L becomes weaker for a load variation higher than 40 Ω. Indeed, considering the previous WF mass flow rate equal to 45 g/s, increasing L from 20 Ω up to 40 Ω the expander speed grows from 2200 RPM up to 2800 RPM. The rapid increase of speed with L observed in this range explains the high reduction rate of expander intake pressure. This is since expander speed produces an increase of expander permeability α (eq.(1)) which expresses the capability of the machine to be crossed by working fluid, [30]. Permeability, indeed, can be evaluated as the ratio between the WF mass flow rate and the expander intake pressure, [30].

$$\alpha = \frac{\dot{m}_{WF}}{p_{exp,in}} \quad \text{(eq.1)}$$

The volumetric expander, in fact, it can be seen as a revolving valve, so, the higher it is the speed, the lower is the pressure difference at its sides for a given working fluid mass flow rate. So, considering that the pressure at expander outlet can be retained constant (it is defined by the cold source properties quite constant for the case at hand), the permeability growth produces a diminution of the expander intake pressure. The permeability growth with L can be noticed in Fig. 5. Here, it can be clearly seen that for a given $\dot{m}_{WF}$ the permeability rapidly increases from 0.044 up to 0.048 kg/(MPa·s) enhancing L from 20 Ω up to 40 Ω, whereas a weaker reduction is noticed for L larger than 40 Ω. This explains the weaker expander intake pressure variation after this value. A direct consequence of permeability increase is the reduction of expander pressure ratio (Fig. 6). In fact, when the permeability raises the expander intake pressure diminishes leading to the decrease of expander pressure ratio, [30].

This observation allows to provide a theoretical explanation about the effect of L variation on plant operability. Indeed, it is known in literature [24–27] when the electrical load decreases, the absorbed current increases leading to a growth of the expander torque and a reduction of expander speed.

As definitive conclusion it appears that.

a) The most important parameter influencing the inlet expander pressure is the WF mass flow rate and L values. For L values greater than 30–40 Ω, the effect of this parameter is weak.

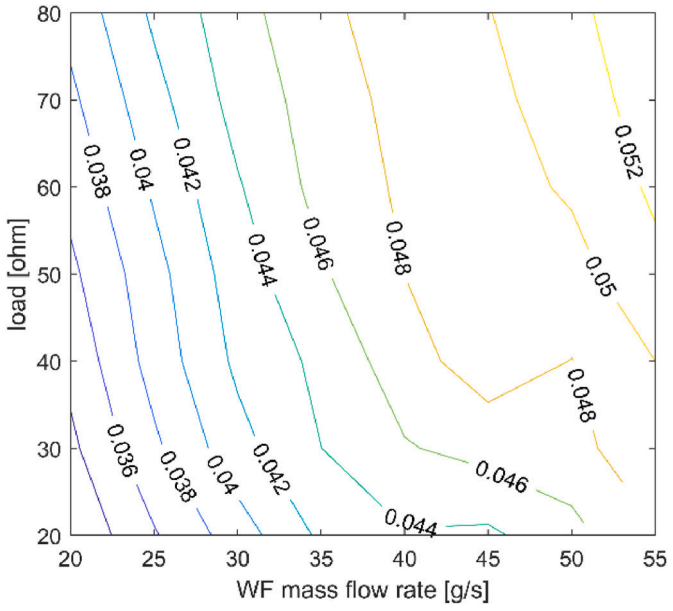

Fig. 5. Experimental expander permeability [kg/(MPa·s)] as function of load resistance and mass flow rate of WF.

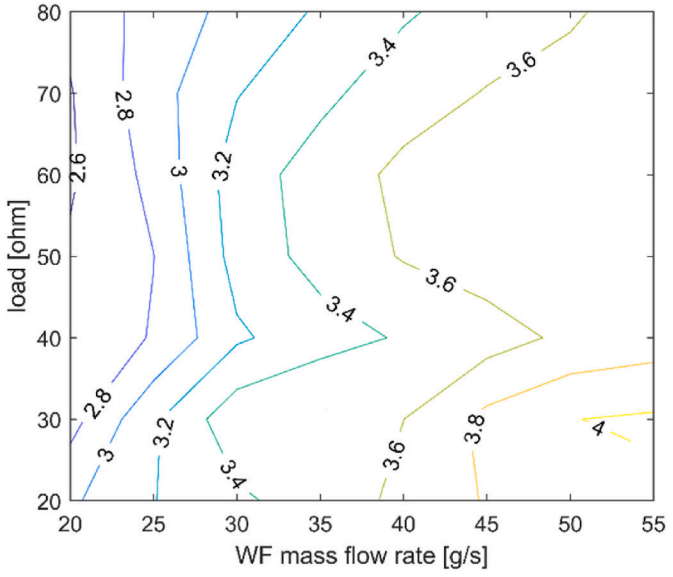

Fig. 6. Experimental pressure ratio as function of load resistance and mass flow rate of WF.

b) L can be used as controlling parameter of the revolution speed of the expander. If WF flow rate increases due to the need of recovering more heat from the hot source, the electric load must be decreased. For a specific unit, the electric load variation vs WF flow rate is inversely proportional and presents a trend which is easily sored in a look-up table.
c) The concept of fluid dynamic permeability allows to understand some relationships between WF flow rate, inlet expander pressure and, therefore, all the properties if the unit which defines the energy performances of the unit. Being the electric load a dominant parameter on the expander speed, its variation is the easiest way to set up the best conditions for the expander.

3.2. Experimental analysis of the effect of electric load and WF mass flow rate on expander performance

The variation on the operating quantities of the unit caused by the load and WF mass flow rate variation produces significant effect on expander, and consequently, on ORC-unit performance. In Fig. 7, the expander power as function of L and WF mass flow rate is shown. Reducing the load resistance for a given WF mass flow rate, the expander power grows. This is results is a consequence of the trend observed for pressure ratio which increases reducing L for a given WF mass flow rate (Fig. 6). On the other side, keeping constant L, the increase of WF mass flow rate produces a growth of expander power. This is due to the increase of pressure ratio with WF mass flow rate (Fig. 6). Therefore, the maximum expander power is observed in correspondence of high WF mass flow rate and low L values. The maximum expander power is equal to 650 W and is achieved in correspondence of 20 Ω and a WF mass flow rate of 55 g/s. Hence, for the considered plant size, setting a WF mass flow rate (for a given thermal power available at evaporator) the expander power increases reducing L. This means that the expander pressure ratio (which increases with L reduction) has greater effect on power than the expander speed (which decreases with L reduction). The expander power (eq.(2.1)) is indeed defined by the difference between the indicated power and the power lost due to friction, [31].

$$P_{exp} = P_{ind} - P_{losses} \quad \text{(eq.2.1)}$$

The indicated power represents the power provided to the machine mobile components by the working fluid and it coincides with the area of the indicated diagram representing the inner chamber pressure trace as function of its volume. Indicated power can be expressed as eq.(2.2), [31]:

$$P_{ind} = \sum_{i=1}^{N} \omega_{exp} \oint p_i dV_i \quad \text{(eq.2.2)}$$

P_{ind} increases with pressure inside the chamber and expander speed. When L diminishes the expander intake pressure grows (Fig. 3) thus enhancing the pressure inside the chamber. This provides an increase of P_{ind} despite the reduction of expander speed (number of cycles per second) caused by L reduction. So, the effect on indicated power of the pressure ratio growth is higher than that of expander speed decrease. Moreover, the expander speed decrese has a positive benefit on friction

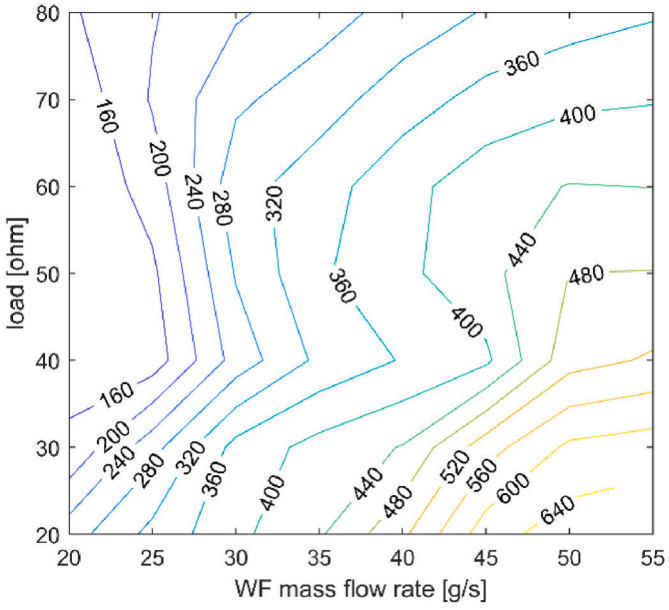

Fig. 7. Experimental expander power [W] as function of load resistance and mass flow rate of WF.

power reduction thus giving another contribution on expander power increase with L reduction.

In terms of expander efficiency (Fig. 8), the maximum value is observed always for electric load resistance of 20 Ω but for lower WF mass flow rate. This is since in this condition a pressure ratio (2.8–3) closer to built-in volume ratio is achieved than cases at higher L and WF mass flow rate. In fact, if the expansion ratio is close to the built-in volume ratio under and over expansions at the expander outlet are minimized.

Expander efficiency was evaluated considering as reference transformation ana adiabatic isentropic expansion (eq.(3)), [30]:

$$\eta_{exp} = \frac{P_{exp}}{\dot{m}_{WF}\left(h_{exp,in} - h_{exp,out,is}\right)} \quad \text{(eq.3)}$$

as it is defined widely in literature even though the denominator does not fully apply to volumetric machines since expansion happens inside a finite volume and the adiabatic isoentropic expansion in not a reference, as it is for dynamic machines.

Fig. 9 introduces the volumetric efficiency of the expander, defined as in equation (4), [30]:

$$\eta_{vol} = \frac{\rho_{exp,in} V_{exp,in} \omega_{exp}}{\dot{m}_{WF}} \quad \text{(eq.4)}$$

It can be observed from Fig. 9 that higher values of volumetric efficiency are achieved for high values of L. This is due to the increase of expander speed (Fig. 4) when L increases. Expander speed growth, as matter of fact, plays a positive effect on the reduction of clearance gap. Moreover, the reduction of pressure ratio achieved simultaneously for high L leads to diminution of volumetric losses. Pressure ratio is indeed the main driver of pressure losses through the clearance gaps, so, its reduction provides positive benefits on volumetric efficiency.

It is worth to be notice that all the analyses were carried out for a comparable superheating degree as observed in Fig. 10. Indeed, for all the considered range, the superheating degree of WF at expander intake varies between 8 °C and 18 °C ensuring and effective starting point for an expansion in gaseous phase. As aforementioned, expander is the key component of the ORC-based power unit, hence, it significantly affects the whole ORC-based power unit performance. Indeed, as it can be observed from Fig. 11, the power produced by the unit reflects the expander power trend. Indeed, the maximum power is achieved for low

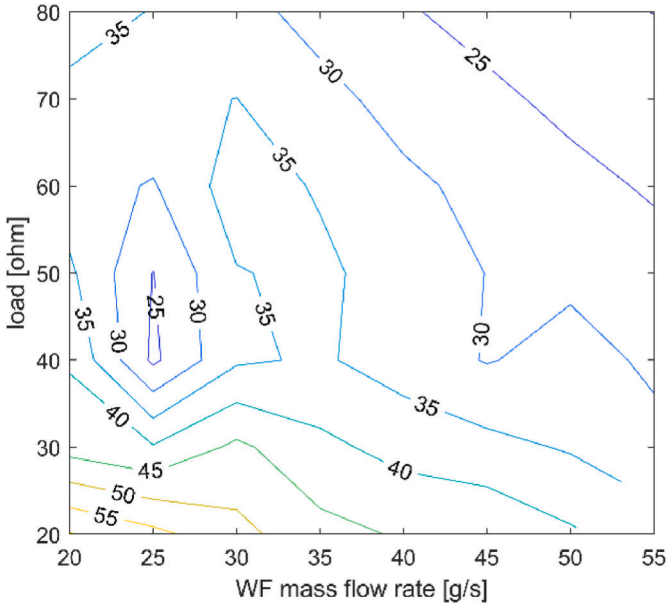

Fig. 8. Experimental expander efficiency [%] as function of load resistance and mass flow rate of WF.

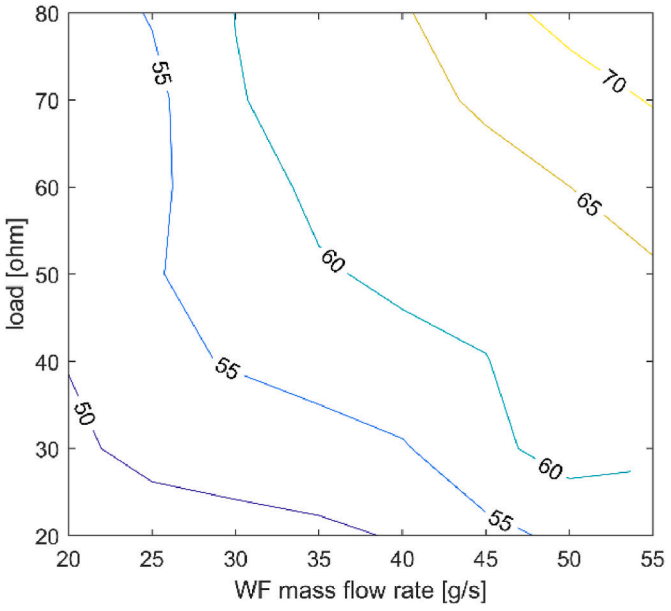

Fig. 9. Experimental expander volumetric efficiency [%] as function of load resistance and mass flow rate of WF.

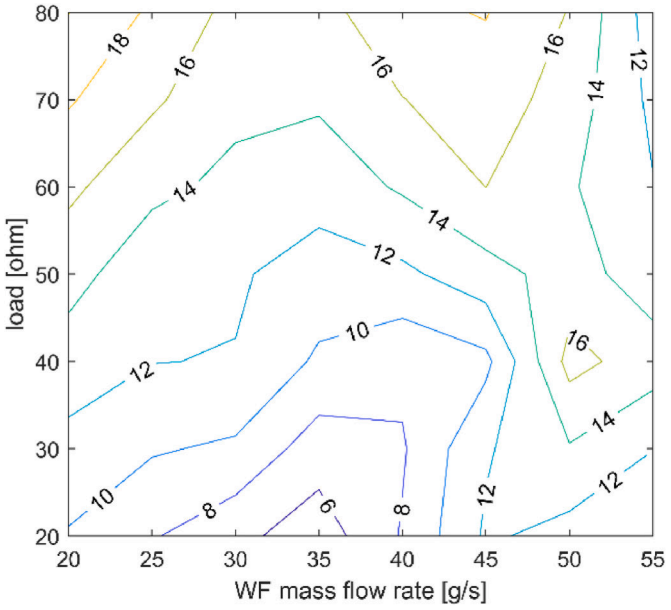

Fig. 10. Experimental superheating degree [°C] at expander inlet as function of load resistance and mass flow rate of WF.

L values and high WF mass flow rates.

An aspect that should be remarked, is that when a low L is considered, also in correspondence of small WF mass flow rate (low thermal power available at evaporator) a significant power can be achieved. Indeed, considering that in correspondence of design point (50 g/s) the produced power is 400 W, if the WF mass flow rate diminishes up to 50 % (25 g/s) the power decrease is limited to 25 % for a load resistance of 20 Ω. This aspect is made possible in this condition thanks to the capability to maintain large expansion ratio also for low WF mass flow rate (Fig. 5).

In Fig. 12, the ORC-based power unit efficiency is reported as defined in equation. (5), [30]:

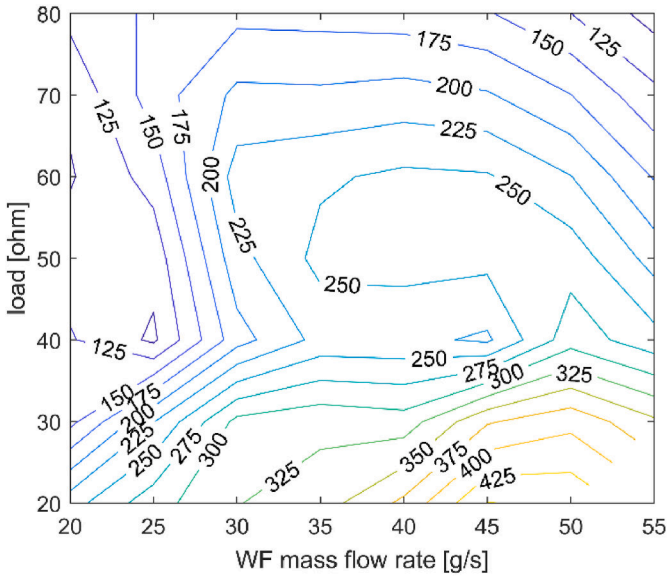

Fig. 11. Experimental ORC-based power [W] as function of load resistance and mass flow rate of WF.

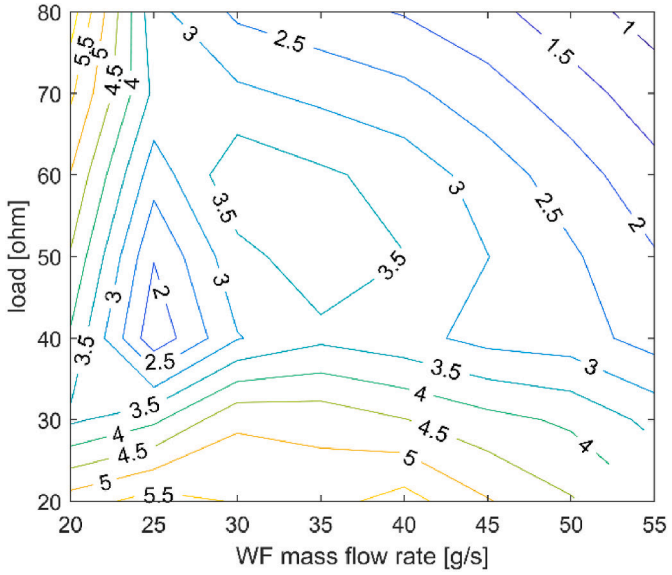

Fig. 12. Experimental ORC-based efficiency [%] as function of load resistance and mass flow rate of WF.

$$\eta_{ORC} = \frac{P_{ORC}}{\dot{m}_{HW} c_{p,HW} \left(T_{HW,in} - T_{HW,out}\right)} \quad \text{(eq.5)}$$

The maximum value (5.5 %), is achieved in correspondence of WF mass flow rate between 20 g/s and 30 g/s. Anyway, in correspondence of L values between 20 Ω and 40 Ω, efficiency changes between 3.5 % and 5.5 % over the whole WF mass flow rate range. Anyway, efficiency for a huge part of the operating range assumes values higher than 2.5 %. This unit presents an efficiency in line with the best literature results [36–38]; the relatively low value is explained by the reduced temperature distance between hot and cold temperature sources.

In Fig. 13, the ORC-based unit operating range was reported in terms of power as function of permeability and hot water temperature at PHRVG inlet. Reducing the hot water inlet temperature, if permeability diminishes, the expander power can be maximized. Indeed, reducing the hot water inlet temperature from 110 °C up to 80 °C, if the permeability diminishes from 0.046 kg/(MPa·s) up to 0.032 kg/(MPa·s) the power

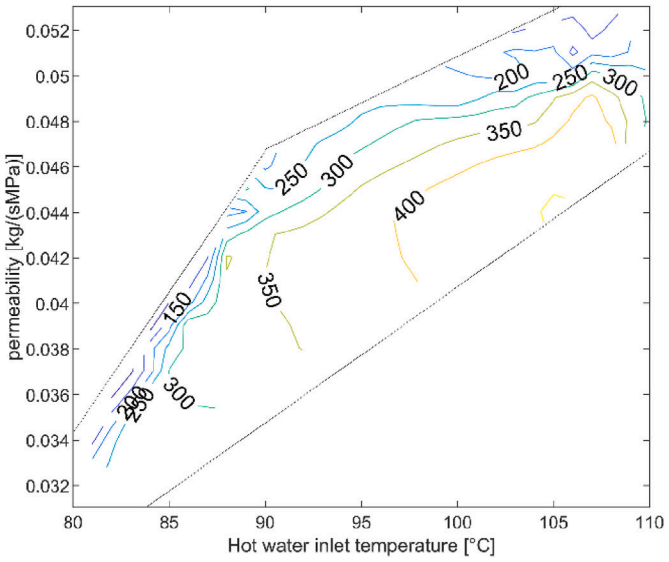

Fig. 13. Experimental ORC-based unit power [W] as a function of hot water temperature and plant permeability.

reduction can be limited in a percentage of 25 % (from 400 W up to 300 W). For higher permeability value, the power reduction presents a high rate with the reduction of the hot water temperature. To associate the permeability value to L and WF mass flow rate Fig. 5 can be used. Indeed, Fig. 5 represents the permeability as function of the L and WF mass flow rate. Hence, Figs. 13 and 5 can be used together as a map to ensure the best power value for each hot water temperature.

In Fig. 14 the efficiency of the unit is reported. It is interesting to observe that decreasing the hot water temperature from 110 °C up to 80 °C, the plant efficiency can vary in a narrow range close to the maximum value (5 %). This can be obtained properly reducing the expander permeability. As for power case (Fig. 13), through the combined observation of Fig. 14 with Fig. 5, WF mass flow rate variation provides the required permeability.

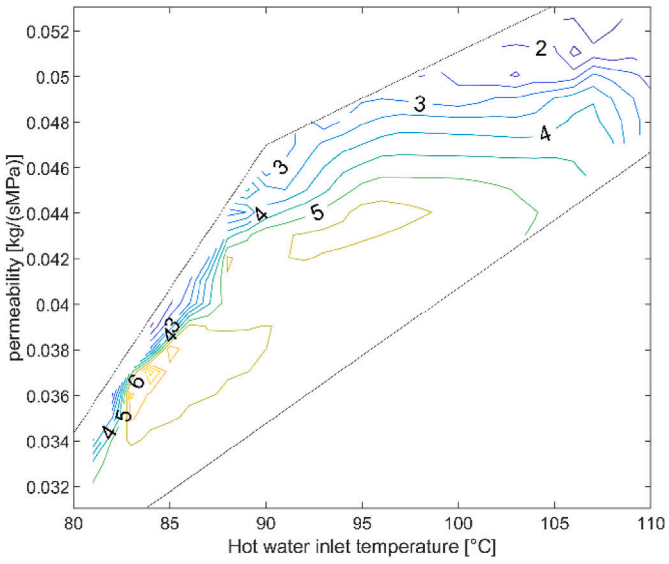

Fig. 14. Experimental ORC-based unit efficiency [%] as a function of hot water temperature and plant permeability.

3.3. Experimental analysis of the effect of electric load and WF mass flow rate on ORC-based unit operating range

The operating range of the unit speed controlled by the electric load was compared with a case in which the same unit operated with a SVRE (of the same power size) mechanically linked with an asynchronous electric generator electrically connected with the grid (50 Hz) and equipped with an inverter which allowed to decouple the expander speed with that imposed by the grid on the electrical machine. Such latter configuration was deeply characterized in authors previous work, [30].

The comparison here performed aims to show the different operating behaviour of the two expander configurations (Fig. 15). Fig. 15 reports on a plane the net power produced by the unit having in the x-axis the hot water inlet temperature to the PHRVG and in the y-axis the fluid dynamic permeability. Iso-power lines are reported; in the top part the performances of the SVRE, in the bottom part the ones given by the scroll expander. In the first case, expander (SVRE) speed is controlled by an inverter regardless the electrical connection of the generator with the grid. In the second case, the speed is varied via the electric load connected to the generator. In Fig. 16 the iso-efficiency lines are reported.

Results reported in Figs. 15 and 16 outline that in case of speed controlled SVRE, the operating range in terms of power and efficiency is wider with respect those achieved with hermetic scroll. Anyway, the power values are significantly higher for scroll expander since this machine, despite have a similar size of SVRE [26], presents a lower permeability. Indeed, the fluid dynamic permeability seen by the scroll expander varies in the range 0.025–0.055 kg/(MPa·s) whereas SVRE presents higher values (0.06–0.11 kg/(MPa·s)). This means that the unit with the scroll expander can work with lower mass flow rate to ensure the same expander pressure difference values with respect to SVRE case.

Such aspect can be seen in Fig. 17 showing the expander pressure difference as function of WF mass flow rate for scroll expander (a), and speed controlled SVRE (b). Considering for instance an expander pressure difference of 8, scroll expander needs a significantly lower mass flow rate (45 g/s) with respect SVRE case (60 g/s). Hence, when a scroll expander is considered (Fig. 18(a)) a similar power of the SVRE (Fig. 18 (b)) can be achieved but with a lower WF mass flow rate. In fact, in these points the scroll expander produces 650 W whereas SVRE 700 W. Anyway, the lower WF mass flow rate of the scroll expander involves a

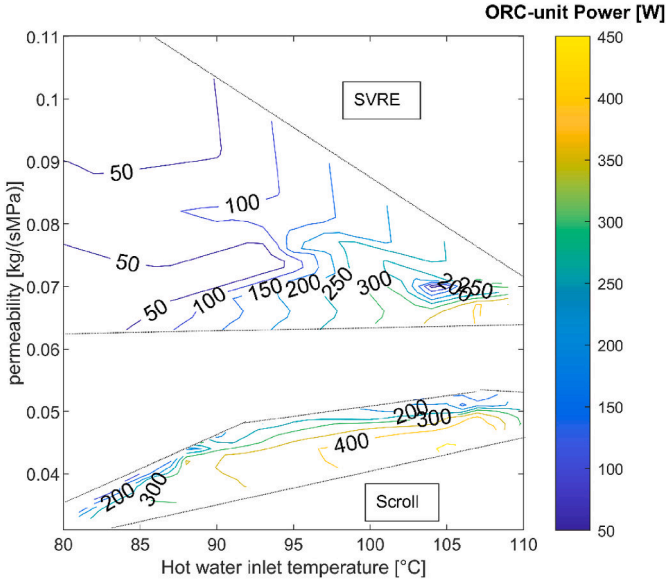

Fig. 15. Comparison between operating range (Power [W]) of ORC-based unit with SVRE and Scroll as function of hot water temperature and plant permeability.

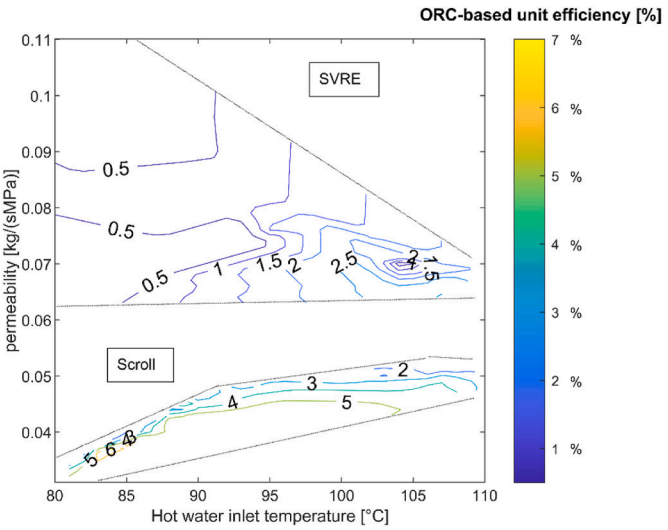

Fig. 16. Comparison between operating range (efficiency [%]) of ORC-based unit with SVRE and Scroll as fucntion of hot water temperature and plant permeability.

lower pump power consumption as can be noticed from the Back Work Ratio (BWR) (eq.(6)) shown in Fig. 19. BWR expresses the ratio between pump and expander power and for the scroll machine (in the considered points) is 25 % (Fig. 19(a)) whereas for SVRE is 45 % (Fig. 19(b)). This explains the reason of the higher net plant power values achieved in case of the use of the scroll, [31].

$$BWR = \frac{P_{pmp}}{P_{exp}} \quad \text{(eq.6)}$$

Such results show that if the expander sees a proper permeability, good performances can be achieved even though the expander speed is not externally set through an inverter. In fact, for the case at hand, the low thermal power of the heat source leads to low WF mass flow rate. Thanks to the lower scroll permeability, large pressure ratios can be ensured even in these conditions. Indeed, for the considered case when L is 20 Ω, for a given WF flow rate higher pressure ratio is achieved with respect to larger L leading to higher power production (Fig. 18(a)). Thus, when L is low, machine presents a low permeability. The permeability increases with the growth of L (40 and 80 Ω) thus enhancing the mass flow rate which can be elaborated for a given pressure ratio. Consequently, when the WF is high due to the growth of heat thermal source, L growth ensures to enhance the machine permeability thus minimizing the expander intake pressure (ORC maximum pressure). So, varying L, the same ORC-based unit could be able to follow the variation of the heat source thermal power. This allows to explain a new perspective in literature.

Indeed, in Ref. [29] it is claimed that to guarantee proper operation of the unit, the electric load resistance should match the expander power output. Hence, the analysis developed in the present research demonstrates what is the impact of load variation on the unit from the point of view of the relation between the main operating quantities (WF mass flow rate and maximum pressure). It should be kept in mind that the variation of L cannot be always possible. Indeed, the electric load resistance in final application is fixed or its variation limited by external factors. Anyway, as Fig. 16 shows, for a given WF mass flow rate range, there is only one value of electric load resistance allowing to optimize the machine performance.

Therefore, if L is properly set “a priori” according to the expected thermal power of heat source (and consequently WF mass flow rate), the unit can operate properly because the expander presents an adequate permeability. Indeed, as it happens for the considered case, despite scroll expander speed is not fixed, it shows a self-regulatory capacity

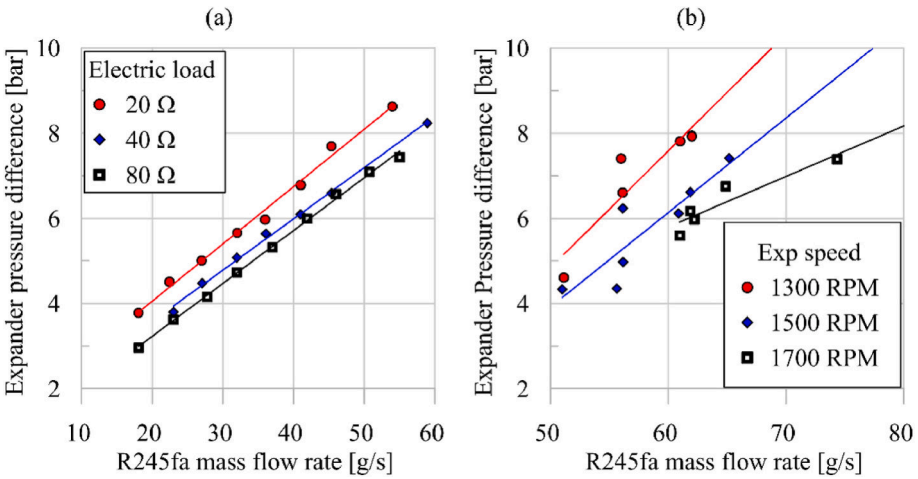

Fig. 17. Expander pressure difference in case of scroll expander connected to resistive electric load (a) and SVRE connected to inverter and electric network (b).

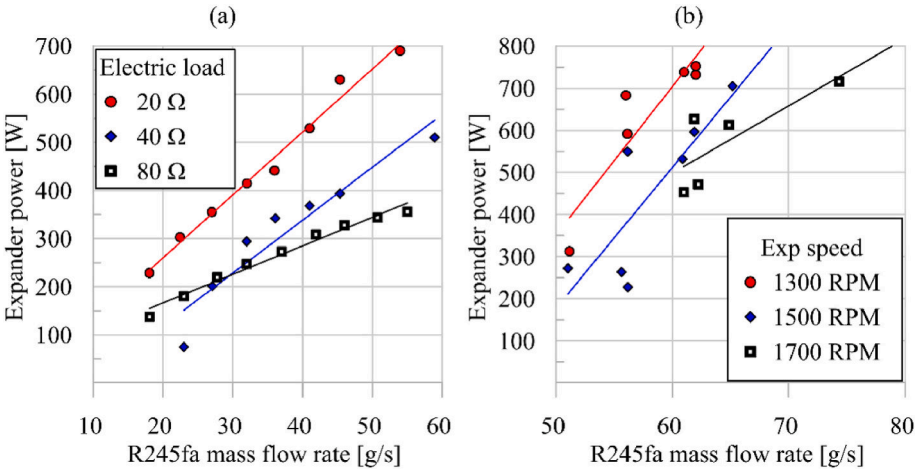

Fig. 18. Expander power in case of scroll expander connected to resistive electric load (a) and SVRE connected to inverter and electric network (b).

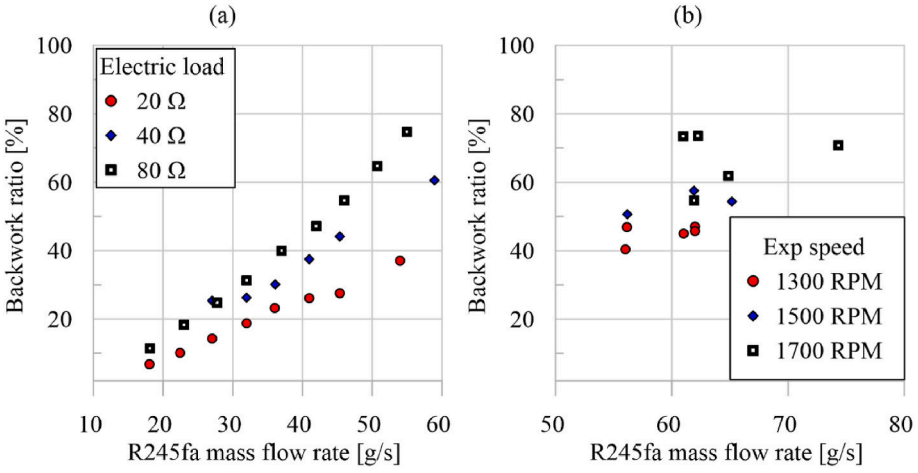

Fig. 19. Backwork ratio in case of scroll expander connected to resistive electric load (a) and SVRE connected to inverter and an electric network (b).

characterized by the linear variation of pressure ratio as function of WF mass flow rate. This aspect is demonstrated by the fact that scroll operating area (Figs. 15 and 16) is inclined with respect to the hot water axis. When hot water temperature diminishes, the unit reduces its permeability without an external speed control. This self-regulatory capability is due to the speed reduction with WF mass flow rate observed when a volumetric machine is connected to a resistive electric load (Figs. 4 and 6). Thus, when the thermal power of hot source decreases forcing the WF mass flow rate to decrease, the reduction of permeability allows to ensure high value of pressure (and consequently

of pressure ratio) thus achieving high expander power production. Indeed, it can be observed that also for low temperature values which justify (20–30) g/s of WF mass flow rate, a power of the order of 200–250 W can be produced.

Differently, for the SVRE case, the operating range appears like a cone (Figs. 15 and 16). When the expander speed can be externally set as in this case, the permeability of the machine can be controlled and the slope of the linear relation between pressure ratio and WF mass flow regulated, [30]. Anyway, even reducing the expander speed, the lower permeability of SVRE involves a smaller pressure ratio of scroll expander. Hence, the external speed control allows to provide a wider permeability variation with respect to the scroll case where the permeability variation is more effective despite it is constrained in a narrower range. This demonstrate that the expander speed should be always associated with a proper expander permeability with respect to the operating range.

Therefore, in case of connection of the expander with an electric load the following observation can be outlined.

- The electric load should be set according to the expander power output, so low electric load should be set for small WF mass flow rate to achieve large pressure ratio;
- A proper expander permeability allows to achieve high performance even if the expander speed is not externally controlled. Indeed, scroll expander present better performance than a more permeable machine (SVRE) despite it is directly speed-controlled. This means that the self-regulatory capacity of the expander allows to operate properly for a certain working range;
- The SVRE external speed control, anyway, allows to widen the machine operability and to further improve its performances; a proper permeability should be defined.

3.4. *Theoretical relation of the effect of the electric load on an ORC-based power unit and operating range increase*

Besides the experimental analysis, a theoretical equation reproducing the relation between all the involved operating quantities is developed. Such relations aim to predict the effect of the variation of the independent variable (WF mass flow rate and expander load) on the plant operability. For a typical configuration involving the connection of expander generator with a resistive load, to the best author knowledge a mathematical representation of the effect of load variation on the main operating parameter (ORC maximum pressure, expansion ratios, WF mass flow rates) is still an open point. Indeed, there are several experimental analyses [24–29] reporting the effect on the plant performance but a theoretical relation allowing quantitatively to reproduce this effect is lacking. Hence, to fill this gap, in the present paper a theoretical analysis was carried out to support and explain the experimental results.

The theoretical model is based on the permeability concept, which defines the attitude of a volumetric expander to be crossed by a working fluid. Authors widely assess this concept for volumetric machine whose speed is externally controlled, [30]. In Ref. [30] authors also represent the case in which the expander is connected to a constant electric load. In this work, the constrain of fixed load was removed and this further degree of freedom was considered making the analysis more comprehensive.

The first step of the model is the same of the permeability theory developed in previous work, [30]. Starting from the expander volumetric efficiency equation (eq.(4)) equation (7) can be achieved, [30]:

$$\dot{m}_{WF} = \frac{\rho_{exp,in} V_{exp,in} \omega_{exp}}{\eta_{vol}} \quad \text{(eq.7)}$$

Rearranging the terms the density of the working fluid at the expander inlet can be represented (eq.(8)), [30]:

$$\rho_{exp,in} = \frac{\eta_{exp}}{V_{exp,in}\omega_{exp}} \dot{m}_{WF} \quad \text{(eq.8)}$$

Combining eq.(8) with the ideal gas relation corrected by compressibility factor (eq.(9)), a relation expressing the relation between the expander intake pressure and working fluid mass flow rate is found (eq.(10)), [30].

$$p_{exp,in} = ZRT\rho_{exp,in} \quad \text{(eq.9)}$$

$$p_{exp,in} = \frac{ZRT\eta_{exp}}{V_{exp,in}\omega_{exp}} \dot{m}_{WF} \quad \text{(eq.10)}$$

This relation, developed by the author in Ref. [30] represent the general permeability equation. Anyway, according to the case considered, between expander speed and the other involved quantities different relation exists.

In fact, for the case in which the expander speed is externally set through an inverter, it is independent from working fluid mass flow rate. On the contrary, when the expander is connected to a resistive load varied in order to change the expander speed, as it was seen in Ref. [30] a linear dependence exists between expander speed and working fluid mass flow rate. This causes that the expander speed is not a degree of freedom, depending on WF mass flow rate. Hence, if the electric load is kept constant, the expander intake pressure (ORC maximum pressure) depends only on the WF mass flow rate.

The situation changes for the case at hand as the electric load resistance variation is considered. Indeed, as literature shows and the present experimental analysis confirms, a variation of this parameter causes a modification of the expander speed for a given working fluid mass flow rate. This means that in the case that the pump speed and the electric load were varied, two degrees of freedom defines the expander intake pressure. Hence, the permeability relation should be integrated considering also this effect which was not considered up to date.

In this way a novel form of the permeability relation can be outlined (eq.(11)):

$$p_{exp,in} = \frac{ZRT\eta_{exp}(L, \dot{m}_{WF})}{V_{exp,in}\omega_{exp}(L, \dot{m}_{WF})} \dot{m}_{WF} \quad \text{(eq.11)}$$

In Fig. 20, it can be seen as the expander intake pressure quite linearly increases as function of WF mass flow rate for a given electric load resistance. More in detail, in correspondence of a given electric load resistance, volumetric efficiency and expander speed present a linear growth with WF mass flow rate as Figs. 21 and 22 respectively show.

This means that for volumetric efficiency and expander speed, two linear fitting equations can be set up (equations (12) and (13)), where slope (k) and the y-axis intercept (q) depend by the electric load

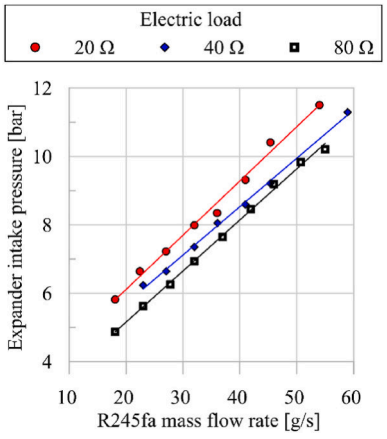

Fig. 20. Experimental expander intake pressure trend as function of WF mass flow rate and electric load.

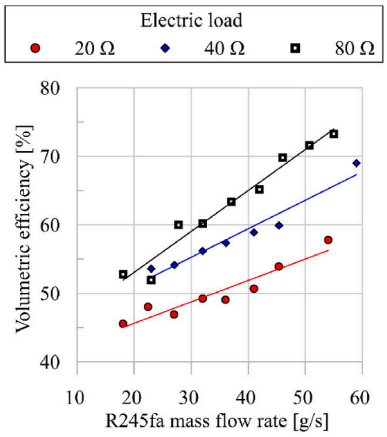

Fig. 21. Experimental volumetric efficiency as function of WF mass flow rate and electric load.

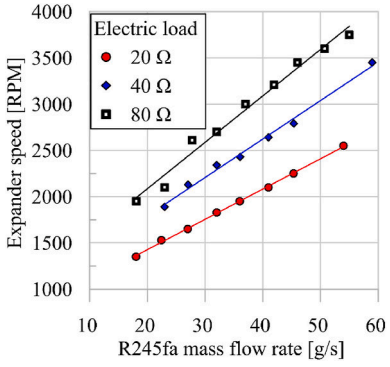

Fig. 22. Experimental expander speed as function of WF mass flow rate and electric load.

resistance (L):

$$\eta_{vol} = k_{\eta}(L)\dot{m}_{WF} + q_{\eta}(L) \quad \text{(eq.12)}$$

$$\omega_{exp} = k_{\omega}(L)\dot{m}_{WF} + q_{\omega}(L) \quad \text{(eq.13)}$$

Equations (12) and (13) express respectively the relation of volumetric efficiency and expander speed on the two degrees of freedom considered. These are the mass flow rate and the electric load. It is important to observe that also the volumetric efficiency presents a dependence on these parameters. Indeed, volumetric efficiency depends on the expander speed for volumetric expanders. This relation represents a novel aspect for the permeability calculation.

In Figs. 23 and 24, k_{η}, k_{ω} and q_{ω} are reported as function of L as the

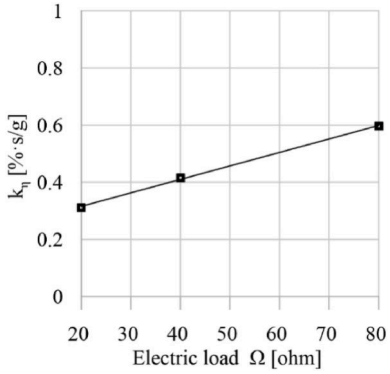

Fig. 23. k_{η} of volumetric efficiency as function of electric load.

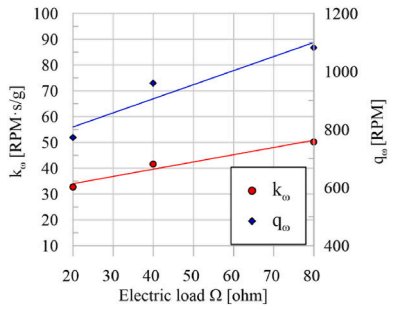

Fig. 24. k_{ω} and q_{ω} of expander speed as function of electric load.

experimental data offer. It can be observed that k_{η}, k_{ω} and q_{ω} linearly increase with electric load resistance as it can be seen in Figs. 23 and 24, respectively. Concerning q_{η} it slightly varies as function of L, hence a constant value equal to 41.1 [%] is assumed from experimental data evaluating the volumetric efficiency in percentage values.

Hence, the linear dependence of k_{η}, k_{ω} and q_{ω} with L can be expressed through equations (14.1), (14.2) and (14.3) respectively:

$$k_{\eta}(L) = k_{\eta L}L + A \quad \text{(eq.14.1)}$$

$$k_{\omega}(L) = k_{\omega L}L + B \quad \text{(eq.14.2)}$$

$$q_{\omega}(L) = k_{q\omega L}L + C \quad \text{(eq.14.3)}$$

where $k_{\eta L}$, $k_{\omega L}$ and $k_{q\omega L}$ are respectively the slope of k_{η} and k_{ω} and q_{ω} with electric load, whereas A, B and C are the corresponding y-axis intercepts. Then, combining equations (12) and (14.1) the volumetric efficiency as function of load resistance and working fluid mass flow rate can be drawn (eq.(15)):

$$\eta_{vol} = (k_{\eta L}L + A)\dot{m}_{WF} + q_{\eta} \quad \text{(eq.15)}$$

It is important to mention that volumetric efficiency is expressed in eq.(15) as a percentage value, hence, in the following symbol [%] is assumed as unit of measurement for volumetric efficiency.

Similarly, combining equations 13 and 14.2 and 14.3 also expander speed can be written as function of electric resistance and working fluid mass flow rate (eq.(16)).

$$\omega_{exp} = [k_{\omega L}L + B]\dot{m}_{WF} + k_{q\omega L}L + C \quad \text{(eq.16)}$$

in Table 2 the fitting parameters are summarized.

Both equations (15) and (16) shows a linear dependence with working fluid mass flow rate and the resistance load, so it can be introduced in the permeability relation (eq.(10)) thus achieving equation (17) which can be solved analytically.

$$p_{exp,in} = \frac{ZRT\,[((k_{\eta L}L + A)\dot{m}_{WF} + q_{\eta})/100]}{V_{exp,in}\left[(k_{\omega L}L + B)\dot{m}_{WF} + k_{q\omega L}L + C\right]}\dot{m}_{WF} \quad \text{(eq.17)}$$

Table 2
Fitting parameters.

Parameter	Value	Unit
$k_{\eta L}$	$4.7 \cdot 10^{-3}$	$\frac{\%\cdot s}{g\cdot\Omega}$
A	$22.15 \cdot 10^{-2}$	$\frac{\%\cdot s}{g}$
q_{η}	41.1	%
$k_{\omega L}$	$28.07 \cdot 10^{-2}$	$\frac{RPM\cdot s}{g\cdot\Omega}$
B	28.4	$\frac{RPM\cdot s}{g}$
$k_{q\omega L}$	4.85	$\frac{RPM}{\Omega}$
C	711.97	RPM

To make consistent equation (17), volumetric efficiency is divided by 100 as equation (15) express volumetric efficiency as a percentage value [%].

Results reported in Fig. 25 confirms the good agreement between experimental and theoretical data, as confirmed by a low Mean Absolute Percentage Error (MAPE) equal to 1.6 %. MAPE is evaluated as in eq. (18), [39]:

$$MAPE = \frac{1}{N}\sum_{i=1}^{N}\frac{y_i - \hat{y}_i}{\hat{y}_i} \quad \text{(eq.18)}$$

where N is number of experimental data and $\hat{y}$ and y_i is the i-experimental data and the corresponding prediction, respectively. Indeed, comparing the experimental and theoretical data of these two quantities MAPE of 3.9 % and 3 % can be achieved for expander speed (Fig. 26) and volumetric efficiency (Fig. 27) respectively.

4. Conclusions

In the present paper the effect of electrical load variation on the operability of a 1 kW scale ORC-based power unit was experimentally and theoretically assessed. The ORC-based unit plant was equipped with a scroll expander connected to an electric generator. They were linked together and the electric load "brakes" the speed of rotation of the common shaft, ensuring the reaching of a steady state value of the shaft. This is the case which happens when the unit charges an electrical battery, representing a load whose variation influences the charging intensity. So, speed of rotation of the expander and of the generator depends on the shaft equilibrium and the electric load resistance was a degree of freedom for the generating unit. Hence, to evaluate the effect of load variation on plant operability, the ORC-based unit performance is assessed varying the WF mass flow rate for different resistance values.

Experimental results show the following conclusions.

- When the electric load resistance is reduced the expander speed diminishes leading to a reduction of expander permeability. This involves a higher pressure ratio for a given WF mass flow rate thus enhancing the power production. When the electric load is 20 Ω the expander power production up to 650 W with an ORC-power of 400 W and a plant efficiency close to 5.5 %.
- Operating with low WF mass flow rate (to match an eventual low heat source temperature) the adoption of small electric load ensures high pressure ratio favoring a higher power production. If a larger heat source at high temperature is considered, the larger WF mass flow rates which can result at the HRVG needs to increase the electric load to increase the expander permeability. Therefore, the electric load resistance should be set according to the expander output power.

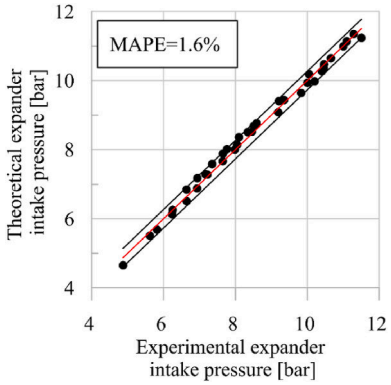

Fig. 25. Comparison between experimental and theoretical expander intake pressure values.

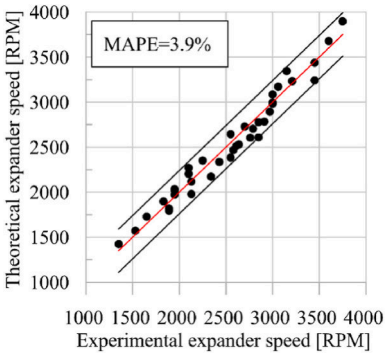

Fig. 26. Comparison between experimental and theoretical expander speed values.

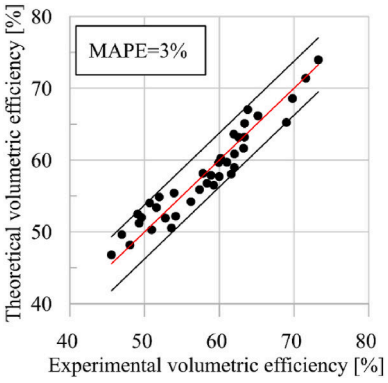

Fig. 27. Comparison between experimental and theoretical volumetric efficiency values.

- A direct speed control allows a wider possibility to vary the pressure ratio for a given WF flow rate. Anyway, the high permeability prevents high power production for low WF mass flow rate. This means that even if the expander speed is not independently controlled as in the scroll case, having the expander a proper permeability and being the electric load matched with the expander power output, the self-regulatory capability of the expander makes the whole unit resilient to severe off-design performances. Indeed, in the scroll case an efficiency close to the maximum value (5 %) can be achieved for most part of the operating range.
- A final contribution of the present work is a theoretical relation allowing to reproduce the impact on electrical load variation on the expander intake pressure, commonly retained the most important regulating parameter. A novel analytical expression has been derived which introduces the electric load charging the generator into a previously derived model by the authors. In this way, a more general and comprehensive model has been developed enriching the capability to use it as tool for the control of the unit.

Nomenclature

Symbols

A-y-axis intercept of the linear variation of k_η with electric load resistance [%·s/g];
B- y-axis intercept of the linear variation of k_ω with electric load resistance [RPM·s/g];
C- y-axis intercept of the linear variation of q_ω with electric load resistance [RPM];
c_p-scpecific heat at constant pressure [kJ/(kgK)]
h-specific enthalpy [kJ/kgK]
$\hat{y}_i$-experimental datum
Z-compressibility factor

Subscripts

(*continued on next page*)

(*continued*)

k_η-slope of the linear variation of volumetric efficiency with working fluid mass flow rate [%·s/g];	BWR-Back-Work ratio
$k_{\eta L}$-slope of the linear variation of k_η with electric load resistance: [%·s/g·Ω];	exp-expander
k_ω-slope of the linear variation of expander speed with working fluid mass flow rate [RPM·s/g];	HW-hot water
$k_{\omega L}$-slope of the linear variation of k_ω with electric load resistance: [RPM·s/g Ω];	i-internal pressure of i-chamber
L-electric load resistance [Ω]	In-inlet
$\dot{m}$-mass flow rate of working fluid [kg/s]-[g/s]	Is-isentropic
N-number of chambers	Ind-indicated
NM- Number of measurements	Losses- power lost due to friction
ORC-Organic Rankine Cycle	Pmp- pump
p-pressure	Out-outlet
P- Power [W]	
PHRVG-Plate Heat Recovery Vapor Generator	vol-volumetric efficiency
q_η- y-axis intercept of linear variation of volumetric efficiency with WF mass flow rate [%·s/g]	
q_ω- y-axis intercept of linear variation of speed with WF mass flow rate [RPM·s/g]	*Greek letters*
$k_{q\omega L}$- slope of the of the linear variation of q_ω with electric load resistance [RPM/Ω];	
R-specific gas constant [kJ/(kgK)]-[J/(kgK)]	α- permeability [kg/(MPa·s)]
V-volume of i-chamber	η-efficiency
WF-working fluid	ρ- density [kg/m^3]
y_i- prediction of experimental datum $\hat{y}_i$	ω-expander speed [RPM]-[RPS]

CRediT authorship contribution statement

Fabio Fatigati: Writing – review & editing, Writing – original draft, Visualization, Validation, Supervision, Software, Methodology, Investigation, Formal analysis, Data curation, Conceptualization. **Roberto Cipollone:** Writing – review & editing, Writing – original draft, Visualization, Validation, Supervision, Project administration, Methodology, Formal analysis, Conceptualization.

Declaration of competing interest

The authors declare that they have no known competing financial interests or personal relationships that could have appeared to influence the work reported in this paper.

Data availability

Data will be made available on request.

Acknowledgements

Authors are grateful to SIVAM S.p.A., SANDEN S.p.A. and Ing. Enea Mattei S.p.A. for the support given during this activity.

References

[1] Serwaa Obobisa Emma, Ahakwa Isaac. Stimulating the adoption of green technology innovation, clean energy resources, green finance, and environmental taxes: the way to achieve net zero CO2 emissions in Europe? Technol Forecast Soc Change 2024;205:123489. https://doi.org/10.1016/j.techfore.2024.123489. ISSN 0040-1625.
[2] Corporate author(s): directorate-general for climate action (European Commission), environment policy and protection of the environment. 2019. ISSN ISBN 978-92-76-02037-0.
[3] The long-term strategy of the United States: pathways to net-zero greenhouse gas emissions by 2050. Published by the United States Department of State and the United States Executive Office of the President, Washington DC November 2021. Designed and Printed by Global Publishing Solutions (U.S. Department of State/A/GIS/GPS). https://www.whitehouse.gov/wp-content/uploads/2021/10/us-long-term-strategy.pdf.
[4] https://japan.kantei.go.jp/101_kishida/statement/202312/01statement.html.
[5] https://ourworldindata.org/grapher/co-emissions-by-sector.
[6] https://www.visualcapitalist.com/a-global-breakdown-of-greenhouse-gas-emissions-by-sector/.
[7] Tian Jinfang, Yu Longguang, Xue Rui, Zhuang Shan, Shan Yuli. Global low-carbon energy transition in the post-COVID-19 era. Appl Energy 2022;307:118205. https://doi.org/10.1016/j.apenergy.2021.118205. ISSN 0306-2619.
[8] Rodriguez-Pastor DA, Becerra JA, Chacartegui R. Adaptation of residential solar systems for domestic hot water (DHW) to hybrid organic Rankine Cycle (ORC) distributed generation. Energy 2023;263(Part D):125901. https://doi.org/10.1016/j.energy.2022.125901. ISSN 0360-5442.
[9] Braimakis Konstantinos, Charalampidis Antonios, Karellas Sotirios. Techno-economic assessment of a small-scale biomass ORC-CHP for district heating. Energy Convers Manag 2021;247:114705. https://doi.org/10.1016/j.enconman.2021.114705. ISSN 0196-8904.
[10] Mascuch Jakub, Novotny Vaclav, Vodicka Vaclav, Spale Jan, Zeleny Zbynek. Experimental development of a kilowatt-scale biomass fired micro – CHP unit based on ORC with rotary vane expander. Renew Energy 2020;147(Part 3):2882–95. https://doi.org/10.1016/j.renene.2018.08.113. ISSN 0960-1481.
[11] Eyerer Sebastian, Dawo Fabian, Schifflechner Christopher, Niederdränk Anne, Spliethoff Hartmut, Wieland Christoph. Experimental evaluation of an ORC-CHP architecture based on regenerative preheating for geothermal applications. Appl Energy 2022;315:119057. https://doi.org/10.1016/j.apenergy.2022.119057. ISSN 0306-2619.
[12] Nazanin Chitgar, Arman Hemmati, Mohtada Sadrzadeh. A comparative performance analysis, working fluid selection, and machine learning optimization of ORC systems driven by geothermal energy. Ener Conv Manag 2023;286:117072. https://doi.org/10.1016/j.enconman.2023.117072.
[13] Energy Convers Manag 2023;286:117072. https://doi.org/10.1016/j.enconman.2023.117072. ISSN 0196-8904.
[14] Xu Xin, Zhang Lian, Zhang Heng, Ma Junlong, Sambatmaryde Kheng. Performance analysis of a novel small-scale integrated solar-ORC system for power and heating. Sol Energy 2024;274:112605. https://doi.org/10.1016/j.solener.2024.112605. ISSN 0038-092X.
[15] Ismail Permana Diki, Azis Mahardika Mohammad, Rusirawan Dani, Farkas István. Utilization of small solar ORC integrated with phase change material in Indonesia condition. J Energy Storage 2024;92:112123. https://doi.org/10.1016/j.est.2024.112123. ISSN 2352-152X.
[16] Fabio Fatigati, Diego Vittorini, Cipollone Roberto. Dynamic response of a micro-scale ORC-based power unit fed by solar flat panels. Appl Therm Eng 2024;243:122546. https://doi.org/10.1016/j.applthermaleng.2024.122546. ISSN 1359-4311.
[17] Zhang Qiang, Feng Yong-Qiang, Xu Kang-Jing, Liang Hui-Jie, Liu Zhi-Nan, Zhao Chuang-Yao, Wang Yong-Zhen, Sapin Paul, Markides Christos N. Dynamic behaviour and performance evaluation of a biomass-fired organic Rankine cycle combined heat and power (ORC-CHP) system under different control strategies. Appl Therm Eng 2024;248(Part B):123236. https://doi.org/10.1016/j.applthermaleng.2024.123236. ISSN 1359-4311.
[18] Wu Jintao, Liang Youcai, Sun Zhili, Zhu Yan, Ye Junhao, Lu Jidong. Dynamic analysis and control strategy of ORC coupled ejector expansion refrigeration cycle driven by geothermal water. J Clean Prod 2024;445:141309. https://doi.org/10.1016/j.jclepro.2024.141309. ISSN 0959-6526.
[19] Wang Jiangfeng, Yan Zhequan, Zhao Pan, Dai Yiping. Off-design performance analysis of a solar-powered organic Rankine cycle. Energy Convers Manag 2014;80:150–7. https://doi.org/10.1016/j.enconman.2014.01.032. ISSN 0196-8904.
[20] Quoilin Sylvain, Aumann Richard, Grill Andreas, Schuster Andreas, Vincent Lemort, Spliethoff Hartmut. Dynamic modeling and optimal control strategy of waste heat recovery Organic Rankine Cycles. Appl Energy 2011;88(6):2183–90. https://doi.org/10.1016/j.apenergy.2011.01.015. ISSN 0306-2619.
[21] Pili Roberto, Wieland Christoph, Spliethoff Hartmut, Haglind Fredrik. Numerical analysis of feedforward concepts for advanced control of organic Rankine cycle systems on heavy-duty vehicles. J Clean Prod 2022;351:131470. https://doi.org/10.1016/j.jclepro.2022.131470. ISSN 0959-6526.
[22] Zhang Xuanang, Wang Xuan, Cai Jinwen, Wang Rui, Bian Xingyan, Yuan Ping, Hua Tian, Shu Gequn. Achieving reasonable waste heat utilization in all truck operating conditions via a dual-pressure organic rankine cycle and its operating strategy. J Clean Prod 2023;419:138302. https://doi.org/10.1016/j.jclepro.2023.138302. ISSN 0959-6526.
[23] Fatigati Fabio, Di Bartolomeo Marco, Battista Davide Di, Cipollone Roberto. Model based control of the inlet pressure of a sliding vane rotary expander operating in an ORC-based power unit. Appl Therm Eng 2021;193:117032. https://doi.org/10.1016/j.applthermaleng.2021.117032. ISSN 1359-4311.
[24] Bianchi M, Branchini L, Casari N, De Pascale A, Melino F, Ottaviano S, Pinelli M, Spina PR, Suman A. Experimental analysis of a micro-ORC driven by piston expander for low-grade heat recovery. Appl Therm Eng 2019;148:1278–91. https://doi.org/10.1016/j.applthermaleng.2018.12.019. ISSN 1359-4311.
[25] Jin Yunli, Gao Naiping, Tong Zhu. Effect of resistive load characteristics on the performance of Organic Rankine cycle (ORC). Energy 2022;246:123407. https://doi.org/10.1016/j.energy.2022.123407. ISSN 0360-5442.
[26] Zhu Jie, Chen Ziwei, Huang Hulin, Yan Yuying. Effect of resistive load on the performance of an organic Rankine cycle with a scroll expander. Energy 2016;95:21–8. https://doi.org/10.1016/j.energy.2015.11.048. ISSN 0360-5442.
[27] Wu Zhu, Pan Deng, Gao Naiping, Tong Zhu, Xie Feibo. Experimental testing and numerical simulation of scroll expander in a small scale organic Rankine cycle system. Appl Therm Eng 2015;87:529–37. https://doi.org/10.1016/j.applthermaleng.2015.05.040. ISSN 1359-4311.

[28] Bracco Roberto, Clemente Stefano, Micheli Diego, Reini Mauro. Experimental tests and modelization of a domestic-scale ORC (organic rankine cycle). Energy 2013; 58:107–16. https://doi.org/10.1016/j.energy.2012.12.016. ISSN 0360-5442.
[29] Tang L, Wang Y-P, Yang P, Weng Y-W. Experimental study of optimal load characteristics of low temperature heat organic ranine cycle power generation. Shanghai Jiaotong Daxue Xuebao/Journal of Shanghai Jiaotong University 2014; 48(9):1268–73.
[30] Fatigati Fabio, Vittorini Diego, Coletta Arianna, Cipollone Roberto. Assessment of the differential impact of scroll and sliding vane rotary expander permeability on the energy performance of a small-scale solar-ORC unit. Energy Convers Manag 2022;269:116169. https://doi.org/10.1016/j.enconman.2022.116169. ISSN 0196-8904.
[31] Fatigati Fabio, Vittorini Diego, Di Bartolomeo Marco, Cipollone Roberto. Experimental and theoretical analysis of a micro-cogenerative solar ORC-based unit equipped with a variable speed sliding rotary vane expander. Energy Convers Manag X 2023;20:100428. https://doi.org/10.1016/j.ecmx.2023.100428. ISSN 2590-1745.
[32] Awadh Almohammadi Bandar, Al-Zahrani Ahmed, Refaey HA, Attia El-Awady, Fouda A. Energy analysis of a novel solar tri-generation system using different ORC working fluids. Case Stud Therm Eng 2023;45:102918. https://doi.org/10.1016/j.csite.2023.102918. ISSN 2214-157X.
[33] Shahrooz Mina, Lundqvist Per, Nekså Petter. Performance of binary zeotropic mixtures in organic Rankine cycles (ORCs). Energy Convers Manag 2022;266: 115783. https://doi.org/10.1016/j.enconman.2022.115783. ISSN 0196-8904.
[34] Lu Pei, Chen Kaihuang, Luo Xianglong, Wu Wei, Liang Yingzong, Chen Jianyong, Chen Ying. Experimental and simulation study on a zeotropic ORC system using R1234ze(E)/R245fa as working fluid. Energy 2024;292:130453. https://doi.org/10.1016/j.renene.2020.05.016. ISSN 0360-5442, https://doi.org/10.1016/j.energy.2024.130453.Tryfon C. Roumpedakis, George Loumpardis, Evropi Monokrousou, Konstantinos Braimakis, Antonios Charalampidis, Sotirios Karellas, Exergetic and economic analysis of a solar driven small scale ORC, Renewable Energy, Volume 157, 2020, Pages 1008-1024, ISSN 0960-1481.
[35] Freeman James, Hellgardt Klaus, Markides Christos N. Working fluid selection and electrical performance optimisation of a domestic solar-ORC combined heat and power system for year-round operation in the UK. Appl Energy 2017;186(Part 3): 291–303. https://doi.org/10.1016/j.apenergy.2016.04.041. ISSN 0306-2619.
[36] Tsai Yu-Chun, Feng Yong-Qiang, Shuai Yong, Lai Jhao-Hong, Leung Michael KH, Wei Yen, Hsu Hua-Yi, Hung Tzu-Chen. Experimental validation of a 0.3 kW ORC for the future purposes in the study of low-grade thermal to power conversion. Energy 2023;285:129422. https://doi.org/10.1016/j.energy.2023.129422. ISSN 0360-5442.
[37] Soulis Konstantinos X, Manolakos Dimitris, Ntavou Erika, Kosmadakis George. A geospatial analysis approach for the operational assessment of solar ORC systems. Case study: performance evaluation of a two-stage solar ORC engine in Greece. Renew Energy 2022;181:116–28. https://doi.org/10.1016/j.renene.2021.09.046. ISSN 0960-1481.
[38] Ancona Maria Alessandra, Bianchi Michele, Branchini Lisa, De Pascale Andrea, Melino Francesco, Peretto Antonio, Poletto Chiara, Torricelli Noemi. Solar driven micro-ORC system assessment for residential application. Renew Energy 2022;195: 167–81. https://doi.org/10.1016/j.renene.2022.06.007. ISSN 0960-1481.
[39] de Myttenaere Arnaud, Golden Boris, Le Grand Bénédicte, Rossi Fabrice. Mean Absolute percentage error for regression models. Neurocomputing 2016;192: 38–48. https://doi.org/10.1016/j.neucom.2015.12.114. ISSN 0925-2312.